Systems/Circuits

Delta Oscillations Coordinate Intracerebellar and Cerebello-Hippocampal Network Dynamics during Sleep

Arturo Torres-Herraez, Thomas C. Watson,* and Laure Rondi-Reig*

Sorbonne Université, Centre National de la Recherche Scientifique, Institut National de la Santé et de la Recherche Médicale, Institut de Biologie Paris Seine, Neurosciences Paris Seine, Cerebellum Navigation and Memory Team, Paris, F-75005, France

During sleep, the widespread coordination of neuronal oscillations across both cortical and subcortical brain regions is thought to support various physiological functions. However, how sleep-related activity within the brain's largest sensorimotor structure, the cerebellum, is multiplexed with well-described sleep-related mechanisms in regions such as the hippocampus remains unknown. We therefore simultaneously recorded from the dorsal hippocampus and three distinct regions of the cerebellum (Crus I, lobule VI, and lobules II/III) in male mice during natural sleep. Local field potential (LFP) oscillations were found to be coordinated between these structures in a sleep stage-specific manner. During non-REM sleep, prominent δ frequency coherence was observed between lobule VI and hippocampus, whereas non-REM-associated hippocampal sharp-wave ripple activity evoked discrete LFP modulation in all recorded cerebellar regions, with the shortest latency effects in lobule VI. We also describe discrete phasic sharp potentials (PSPs), which synchronize across cerebellar regions and trigger sharp-wave ripple suppression. During REM, cerebellar δ phase significantly modulated hippocampal theta frequency, and this effect was greatest when PSPs were abundant. PSPs were phase-locked to cerebellar δ oscillation peak and hippocampal theta oscillation trough, respectively. Within all three cerebellar regions, prominent LFP oscillations were observed at both low (δ, <4 Hz) and very high frequencies ($\sim$250 Hz) during non-REM and REM sleep. Intracerebellar cross-frequency analysis revealed that δ oscillations modulate those in the very high-frequency range. Together, these results reveal multiple candidate physiological mechanisms to support "offline," bidirectional interaction within distributed cerebello-hippocampal networks.

Key words: cerebellum; delta oscillations; hippocampus; phasic sharp potentials; sleep

Significance Statement

Sleep is associated with widespread coordination of activity across a range of brain regions. However, little is known about how activity within the largest sensorimotor region of the brain, the cerebellum, is both intrinsically organized and links with higher-order structures, such as the hippocampus, during sleep. By making multisite local field potential recordings in naturally sleeping mice, we reveal and characterize multiple sleep stage-specific physiological mechanisms linking three distinct cerebellar regions with the hippocampus. Central to these physiological mechanisms is a prominent δ (<4 Hz) oscillation, which temporally coordinates both intracerebellar and cerebello-hippocampal network dynamics. Understanding this distributed network activity is important for gaining insight into cerebellar contributions to sleep-dependent processes, such as memory consolidation.

Received July 20, 2021; revised Dec. 14, 2021; accepted Dec. 19, 2021.

Author contributions: A.T.-H. and T.C.W. performed research; A.T.-H. and T.C.W. analyzed data; A.T.-H. and T.C.W. wrote the first draft of the paper; L.R.-R., A.T.-H., and T.C.W. edited the paper; T.C.W. and L.R.-R. designed research; L.R.-R. contributed unpublished reagents/analytic tools.

This work was supported by Fondation pour la Recherche Médicale DEQ20160334907; National Agency for Research ANR-17-CE16-0019-SynPredict, ANR-10-LABX-BioPsy, and ANR-11-IDEX-0004-02; Centre National de la Recherche Scientifique, Institut National de la Santé et de la Recherche Médicale; and Sorbonne University to L.R.-R. We thank all members of the Cerebellum Navigation and Memory Team for helpful discussions of the experiments and manuscript; and Institut de Biologie Paris Seine animal facility staff for support.

A. Torres-Herraez' present address: Department of Psychiatry, Columbia University Medical Center, New York, NY 10032.

T. C. Watson's present address: Center for Discovery Brain Sciences, Universit of Edinburgh, Edinburgh, United Kingdom; Simons Initiative for the Developing Brain, University of Edinburgh, Edinburgh, United Kingdom; Patrick Wild Center for Autism Research, University of Edinburgh, Edinburgh, United Kingdom.

*T.C.W. and L.R.-R. contributed equally to this work.

The authors declare no competing financial interests.

Correspondence should be addressed to Laure Rondi-Reig at laure.rondi-reig@sorbonne-universite.fr.

https://doi.org/10.1523/JNEUROSCI.1479-21.2021

Introduction

Many important physiological processes are associated with sleep, including memory formation and consolidation (Diekelmann and Born, 2010; Geva-Sagiv and Nir, 2019). In particular, sleep-related neurophysiological events in the hippocampus, such as place cell reactivations and high-frequency sharp-wave ripples (SWRs) are vital to spatial memory formation (e.g., de Lavilléon et al., 2015). Additionally, widespread slow wave oscillations are thought to play a crucial role in the temporal coordination of discrete sleep-related events, such as hippocampal ripples and thalamo-cortical spindles, across a large network of brain regions (e.g., Nicola and Clopath, 2019)

Recent studies have shown that, during wakeful behavior, the cerebellum is crucial for hippocampal place cell stability and efficient navigation (Burguière et al., 2005; Rochefort et al., 2011;

Babayan et al., 2017; Lefort et al., 2019). Furthermore, the neuroanatomical connectivity required to support this influence has been recently described and physiological correlates of cerebello-hippocampal interaction identified "online" during goal-directed navigation (Watson et al., 2019). So far, however, nothing is known about possible "offline" cerebello-hippocampal physiological interactions during sleep.

To date, sleep research has primarily focused on state-dependent correlation in neocortical and subcortical structures. However, early studies in epileptic patients implanted with intracerebellar electrodes (Niedermeyer and Uematsu, 1974), and recent work using noninvasive techniques (Kaufmann et al., 2006; Schabus et al., 2007; Jahnke et al., 2012) have described state-dependent modulation of cerebellar activity during sleep in humans. During non-rapid eye movement (non-REM) sleep, coordinated slow oscillations, recorded predominantly in cerebellar vermis and fastigial nucleus (Niedermeyer and Uematsu, 1974; Schabus et al., 2007), are correlated with neocortical K-complexes (Jahnke et al., 2012) and sleep spindles (Schabus et al., 2007). During REM sleep, an increase in BOLD signals has been observed in both the cerebellar vermis and hemispheres (Braun, 1997).

Similarly, single-cell recording in animal models has revealed sleep state-related changes in both Purkinje cell and deep cerebellar nuclei neuron firing. During non-REM, no clear neuronal firing rate changes were observed either in cats (Marchesi and Strata, 1970; Hobson and McCarley, 1972; McCarley and Hobson, 1972; Palmer, 1979) or monkeys (Mano, 1970). However, a reduced probability for short interspike intervals was observed in Purkinje cell simple spike firing (McCarley and Hobson, 1972). Consistent with observations made in humans, during REM sleep a significant increase in the firing rate of Purkinje cells was observed in the cerebellar cortex of cats (Marchesi and Strata, 1970; Hobson and McCarley, 1972) and monkeys (Mano, 1970). The presence of large amplitude, phasic events in the cerebellum of cats (Harlay et al., 1974; Pellet and Harley, 1977) and rats (Marks et al., 1980), mainly during REM sleep epochs, has also been attributed to the transmission of ponto-geniculo-occipital (PGO) waves (Farber et al., 1980; Velluti et al., 1985). Finally, recent studies have highlighted cerebellar roles in the generation of sleep spindles in monkeys (Xu et al., 2020) and sleep-wake transitions in mice (Zhang et al., 2020).

Thus, in addition to the multitude of studies highlighting the functional importance of sleep state-dependent processes in the hippocampus (for review, see Klinzing et al., 2019), the aforementioned evidence indicates clear cerebellar activity modulation during sleep (for review, see Canto et al., 2017). Nevertheless, our understanding of spatial and temporal organization of cerebellar activity across sleep states remains rudimentary. Furthermore, to the best of our knowledge, nothing is known about the physiological links between cerebellum and hippocampus during sleep. We therefore simultaneously recorded spontaneous local field potentials (LFPs) from the dorsal hippocampus, vermal cerebellar lobules II/III (Lob II/III), VI (Lob VI), and hemispheric Crus I in freely behaving and sleeping mice. Our analysis reveals that δ oscillations, along with associated phasic sharp potentials (PSPs), temporally coordinate both local cerebellar and distributed cerebello-hippocampal network dynamics in a sleep state-dependent manner.

Materials and Methods

Mice. Twenty adult male C57BL6-J mice were used for this study (Janvier, France; for recordings obtained per animal, see Table 1). Mice were housed individually under a 12 h light/12 h dark cycle (light cycle beginning at 8:00 A.M.) and received food and water *ad libitum*. All behavioral experiments were performed in accordance with the official European guidelines for the care and use of laboratory animals (86/609/EEC) and in accordance with the Policies of the French Committee of Ethics (Decrees no. 87-848 and no. 2001-424). The animal housing facility of the laboratory where experiments were made is fully accredited by the French Direction of Veterinary Services (B-75-05-24; May 18, 2010). The protocol was approved by the Committee on the Ethics of Animal Experiments (APAFIS#4315-2016042708195884v1). Data obtained from the mice used in this study have been published in Watson et al. (2019).

Table 1. Recordings obtained per animal

Animal ID	Lob VI	Lob II/III	Crus I	Hippocampus left	Hippocampus right
J02	+	+	+	+	+
J06	+	+	+	+	+
J07	–	+	–	–	+
J08	+	+	+	+	+
J09	+	+	–	+	+
J10	+	–	–	+	+
J12	+	+	–	+	+
798	+	–	–	+	+
800	+	–	–	+	+
802	+	–	–	+	+
J13	+	+	+	+	+
J15	–	+	+	+	+
J16	+	–	–	–	+
J18	–	–	+	–	+
J19	+	+	+	+	+
J20	–	+	+	+	+
J22	+	–	–	–	+
J23	+	–	+	+	+
J24	–	+	+	–	+
J25	+	–	+	+	–

+/–, recordings were (+) or were not (–) obtained from the listed brain region.

Surgery. Surgical and implant procedures have been already described by Watson et al. (2019). Briefly, surgical implantation was performed under constant isoflurane anesthesia (1.5%) combined with oxygen (1.5 L/min). Animals were placed in a stereotaxic frame device (David Kopf Instruments), and an incision was performed to expose the scalp. Coordinates for implantation were calculated from bregma following the references given in Franklin and Paxinos (2007). We targeted bilateral hippocampi (CA1 region; AP −2.2 mm, ML 2.0 mm, DV 1.0 mm), cerebellar Lob II/III (AP −5.52 mm, ML 0 mm, DV 1.8 mm), cerebellar Lob VI (AP −6.72 mm, ML 0 mm, DV 0.1 mm), and left cerebellar Crus I (AP −6.24 mm, ML 2.5 mm, DV 0.1 mm). Small craniotomies were performed over the target regions using a drill, and the dura was carefully removed with a needle. Two wires of 140-μm-diameter Teflon-coated stainless steel (A-M System) were twisted together to create bipolar LFP recording electrodes (interpolar distance ~0.5 mm) and were implanted in the brain. Pairs of flexible stainless-steel wires were also sutured to the neck muscles to obtain EMG recordings (Cooner Wire). Fourteen mice were also implanted with bipolar stimulation electrodes (same as the LFP electrodes but with interpolar distance of ~140 μm) in the left medial forebrain bundle (AP −1.4 mm, ML 1.2 mm, DV 4.8 mm) to serve as a reward signal in a set of experiments already published (Watson et al., 2019). All electrodes were attached to an electrode interface board (EIB-18, Neuralynx), and the assembly was fixed to the skull using a combination of UV-activated cement (SpeedCem, Henry Shein), SuperBond (SunMedical), and dental cement (Simplex Rapid, Kemdent). Four miniature screws (Antrin) were also attached to the skull for additional support, and an additional screw was attached to the skull over the cerebellum to serve as recording ground. Animals were given a minimum of 5 d post-surgery recovery time before experiments commenced.

Electrophysiological recordings. The EMG and LFP recordings were obtained via a unity-gain headstage preamplifier (HS-18, Neuralynx) and a Digital Lynx SX system and Cheetah software (Neuralynx). Signals were bandpass-filtered between 0.1 and 600 Hz and sampled at 1 kHz. Mouse position was tracked at 30 Hz using video tracker software and

Table 2. Ipsilateral and contralateral cerebello-hippocampus coherence values during non-REM and REM epochs

Sleep state	Frequency band (Hz)	Lob VI - HPC left	Lob VI - HPC right	Lob II/III -HPC left	Lob II/III - HPC right	Crus I - HPC left	Crus I - HPC right
Non-REM	0.1-4	0.534 ± 0.015	0.546 ± 0.020	0.492 ± 0.012	0.491 ± 0.012	0.485 ± 0.009	0.483 ± 0.007
	6-12	0.479 ± 0.004	0.476 ± 0.003	0.475 ± 0.004	0.476 ± 0.004	0.481 ± 0.009	0.475 ± 0.006
	100-200	0.457 ± 0.001	0.456 ± 0.001	0.456 ± 0.001	0.456 ± 0.001	0.457 ± 0.001	0.457 ± 0.001
	240-280	0.458 ± 0.001	0.458 ± 0.001	0.457 ± 0.001	0.458 ± 0.001	0.456 ± 0.001	0.457 ± 0.001
REM	0.1-4	0.499 ± 0.006	0.499 ± 0.007	0.486 ± 0.003	0.491 ± 0.004	0.480 ± 0.004	0.489 ± 0.07
	6-12	0.499 ± 0.004	0.506 ± 0.008	0.489 ± 0.006	0.491 ± 0.005	0.490 ± 0.010	0.493 ± 0.012
	100-150	0.458 ± 0.001	0.458 ± 0.001	0.458 ± 0.001	0.457 ± 0.001	0.458 ± 0.001	0.458 ± 0.001
	250-350	0.459 ± 0.001	0.458 ± 0.001	0.461 ± 0.001	0.460 ± 0.001	0.459 ± 0.001	0.459 ± 0.001

infrared LEDs attached to the headstage (Neuralynx). Recordings were obtained in a bipolar fashion via the Neuralynx software by referencing between the two poles within each electrode.

Histology. After completion of the experiments, mice were deeply anesthetized with ketamine/xylazine solution (150 mg/kg), and electrolytic lesions were created by passing a positive current through the electrodes (30 μA, 10 s). The animals were then perfused transcardially with saline (0.9%) followed by PFA (4%). Once perfused, the electrode assembly was carefully removed, the brain extracted and postfixed in PFA (4%) for 24 h, and then embedded in agarose (3%); 50 μm sagittal and coronal sections for the cerebellum and the hippocampus, respectively, were made using a vibratome. The sections were mounted on gelatinized slides and stained with cresyl violet. The electrolytic lesions were then identified to reconstruct the recording locations using standard maps with reference to a stereotaxic atlas (Franklin and Paxinos, 2007). The anatomic location of the electrodes used in this study was verified by Watson et al. (2019). Recordings were only used if electrode position was positively verified (for summary of recordings obtained per animal, see Table 1).

Behavior and sleep scoring. The animals were recorded during the day (between 10:00 A.M. and 6:00 P.M.) in their home-cages (30 cm × 10 cm × 10 cm), with the lid removed and the lights off for periods up to 4 h. Recordings were made before training in a linear track task (described by Watson et al., 2019). The home-cage environment was familiar to the mice as they had been housed in it since completion of implantation surgery. Animals exhibited different behavioral states that were scored offline and included in four categories: active wakefulness, resting, non-REM sleep, and REM sleep. The scoring was semiautomatically performed using multiparameter thresholds based on instantaneous speed, neck EMG (rectified, smoothed with 1 s window and *z*-scored), and theta/δ ratio in the hippocampal LFP (*z*-scored and calculated in 100 ms bins). Thus, epochs of >4 s with instantaneous speed >3 cm/s were considered as active wakefulness, periods of <30 s where the speed stayed <3 cm/s and were surrounded by active wakefulness epochs were considered as rest. Similarly, when the EMG recording was optimal, a manually selected threshold was also used to discriminate between rest and sleep epochs. We finally used manual thresholding of the theta/δ ratio to separate non-REM and REM sleep epochs. Only epochs of >4 s were selected for further analysis. For subsequent spectral analysis based on sleep scoring, we normalized data duration relative to the sleep state epoch of shortest duration. For example, if 2 min of REM sleep was present in a recording, we randomly selected 2 min of non-REM/wake to make a normalized comparison.

Data preprocessing. All the data processing was performed using custom-made MATLAB scripts (The MathWorks). Raw signals were preprocessed by applying a notch filter to remove electrical line noise (filter centered to 50 Hz). Voltages were *z*-scored to reduce overall differences in amplitude in the signal recorded from different electrodes.

Offline detection of ripples, slow oscillations, and phasic events. Discrete SWRs were detected using criteria used previously (Maingret et al., 2016). The raw signal was then filtered using a second-order zero-phase bandpass filter between 150 and 250 Hz, squared, smoothed (using 8 ms running average), and *z*-scored. The SWRs were defined as events in which the transformed signal remained >2 *z* scores for 30-100 ms with a peak >5 *z* scores.

Slow oscillations in the cerebellum were divided into individual cycles, which were identified as follows: first, the raw signal was filtered using a second-order zero-phase bandpass filter between 0.1 and 4 Hz. The instantaneous phase was obtained by applying a Hilbert transform to the filtered signal. Each cycle was defined by the epoch between two negative peaks on the cosine of the instantaneous phase. Only cycles that lasted >1 s and presented peak amplitudes >4 *z* scores and trough amplitudes no lower than 2 *z* scores were further analyzed.

For the detection of PSPs (putative p-waves) in the cerebellum, we first filtered the signal using a second-order zero-phase bandpass filter between 5 and 80 Hz, squared it, and then calculated the *z* score across all obtained sleep epochs. A double threshold strategy was then applied, first to the transformed signal so that epochs separated by at least 75 ms with values >1 *z* score and a peak in the filtered data >4 *z* scores were considered as events.

Spectral analysis. All the spectral analyses were performed using freely available signal processing toolboxes. For computing the overall spectral power and spectral coherence across sleep states, a multitaper Fourier transform (Chronux toolbox) was computed with 4 s sliding windows in 1 s steps and using four tapers. The mean power spectrum and coherence were obtained for each behavioral state by averaging the spectrogram and coherogram from the identified epochs. To reduce the impact of the different data durations for each state, we split the epochs to match with the minimal data duration, and then we averaged them. For computing the triggered spectrogram and coherograms, we used the continuous wavelet transform and wavelet coherence (wavelet toolbox, MATLAB). We used analytic Morse wavelets with 8 octaves and 48 voices per octave. For coherence analysis, we used the average of both left and right hippocampus: cerebellar site pairings. Coherence values obtained between cerebellum and left or right hippocampus, respectively, are shown in Table 2.

Phase-locking of phasic events and slow-wave triggered power spectra and coherograms. Cerebellar and hippocampal signals were filtered using a second-order zero-phase bandpass filter between 0.1-4 Hz and 6-12 Hz, respectively. The instantaneous phase of the cerebellar infra-slow oscillations and the hippocampal theta oscillations were obtained by applying a Hilbert transform to the filtered signals. The phase-locking of the detected cerebellar phasic events to these rhythms was tested using circular statistics (MATLAB), and significance was determined as Raleigh test p-value < 0.05.

To compute the cerebellar slow wave-triggered spectrogram and coherogram, for each cerebellar slow wave, the obtained time-frequency series was matched with the corresponding instantaneous phase of the cerebellar δ oscillations (0.1-4 Hz) and then averaged by phase bins of 7.35°.

To analyze the impact of PSPs on intracerebellar and cerebello-hippocampal cross-frequency modulation, we classified individual cerebellar δ oscillations in three categories depending on their content of PSPs: no PSPs, when no PSP was detected during the span of the δ wave; isolated PSPs, when PSPs were detected but the intervals between them were larger than 1 s; or clustered PSPs when at least two of them were separated by <1 s.

Cross-correlation between PSPs and SWRs. The timing of the SWRs was calculated relative to the time of the peak of the detected PSPs. After binning at 25 ms resolution, the probability density function (count normalized by the total number of elements multiplied by the bin width) was obtained and smoothed (using a 250 ms running average). Statistical significance of the obtained cross-correlation was performed by

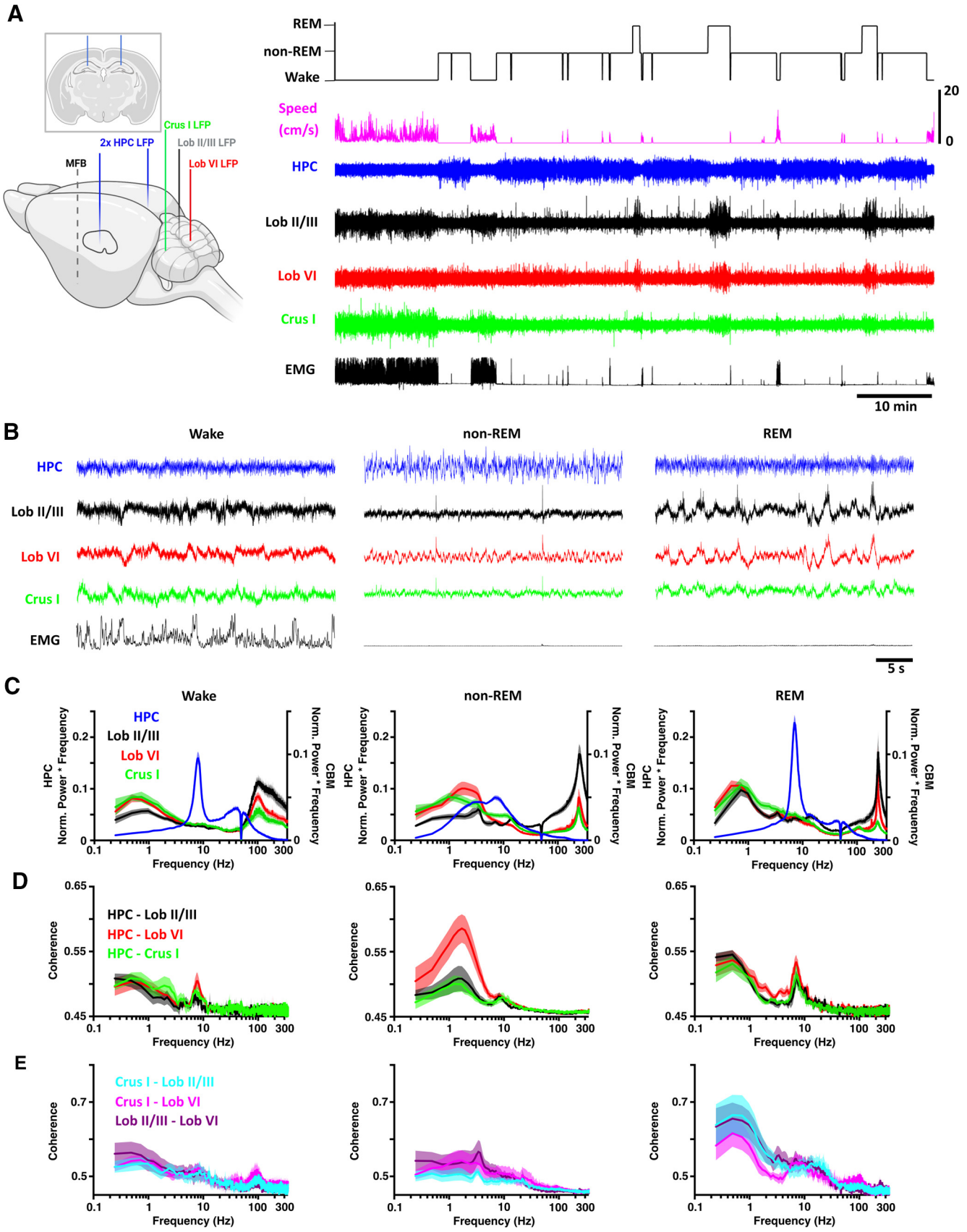

Figure 1. Sleep state-specific activity patterns are present in the cerebello-hippocampal network. ***A***, Left, Schematic illustration of all electrode implantation locations with coronal schematic of hippocampal electrodes as inset. Right, Hippocampal (HPC) and cerebellar cortical (Crus I, Lob VI, and Lob II/III) LFPs were recorded as mice cycled between defined wake, non-REM, and REM states. Created with www.BioRender.com. ***B***, During wake, hippocampal theta and cerebellar $<$1 Hz and high γ (100-160 Hz) oscillations occurred concomitantly. Similarly, during REM, hippocampal theta oscillations were accompanied by widespread δ ($<$4 Hz) and very fast ($\sim$250 Hz) cerebellar oscillations. During non-REM, high-amplitude hippocampal activity co-occurred

artificially generating PSP trains of similar density as observed in the actual data, drawn at random from a Poisson distribution, and recomputing the probability density function.

Statistical analysis. Statistical analyses were conducted using MATLAB Statistical Toolbox and Prism (GraphPad). Normality was assessed using a Shapiro–Wilk test. Parametric and nonparametric tests were then used accordingly. Paired analyses were used when possible. Detailed statistical information is provided in Extended Data Figure 2-1.

Results

Spectral profiling of cerebellar and hippocampal activity across sleep states

We recorded mice in their home-cages across the sleep cycle during a period of ~2 h (141 ± 14 min) and classified their behavior as wake (50.76 ± 7.65 min, obtained from 10 ± 2 epochs), non-REM sleep (81.06 ± 9.27 min, obtained from 19 ± 3 epochs), or REM sleep (9.22 ± 1.38 min, obtained from 12 ± 2 epochs) based on a combination of behavioral and electrophysiological markers (see Materials and Methods). Hippocampal LFP was dominated by sustained, low-amplitude theta oscillations (6-12 Hz) during wake and REM states, and high-amplitude slow oscillations in the δ range (<4 Hz) during non-REM sleep (Fig. 1*A–C*). Conversely, high-amplitude low-frequency oscillations (including < 4 Hz δ waves) were characteristic of wake, REM, and non-REM states in the cerebellum (Fig. 1*A–C*). However, differences in δ oscillation power, as well as peak frequency, were observed both across cerebellar subregions and wake/sleep states (Figs. 1*C*, 2). Similarly, a significant shift in the peak δ frequency was observed during non-REM sleep, specifically in Lob VI (Fig. 2*B*). In contrast, these differences were not observed during REM, when similar spectral profiles were found across cerebellar regions (Fig. 2*B*). Moreover, δ oscillations were highly coherent between cerebellar recording sites (Fig. 1*E*), suggesting that they may play a role in intracerebellar coordination during REM sleep.

In addition to δ activity during wake, high-frequency oscillations (100-160 Hz) were also observed in the cerebellar power spectra (Fig. 1*C*). However, during both non-REM and REM states, power in the high-frequency range was overshadowed by a prominent, narrowband ~240-280 Hz oscillation (classified as very high-frequency oscillations [VHFOs]; Figs. 1*C*, 2*C*,*D*) (de Solages et al., 2008). Local variability within this frequency band was observed across cerebellar regions and sleep states, with maximal values observed in Lob II/III during non-REM and REM sleep (Fig. 2*D*). In contrast, Crus I VHFO power was particularly reduced in REM (Figs. 1*C*, 2*D*, paired *t* tests: Crus I: $n = 11$, $p = 0.0005$; Lob II/III, $n = 11$, Crus I, $n = 11$; Lob VI, $n = 15$; Lob II/III, $n = 11$ mice).

Overall, these data illustrate the presence of lobule and sleep state-dependent LFP dynamics across anterior (Lob II/III), posterior (Lob VI), and hemispheric (Crus I) cerebellum and highlight the existence of a prominent cerebellar δ oscillation.

Cerebello-hippocampal coherence across sleep states

Next, we sought to measure the level of functional coupling (measured as coherence) (compare Watson et al., 2019; Xu et al., 2020) between the cerebellum and hippocampus during wake/sleep states (Fig. 1*D*,*E*). During wake, coherence peaks were similarly observed across δ and theta frequencies in all cerebello-hippocampal combinations (Fig. 1*D*, left). Strikingly, as mice moved to non-REM sleep, δ band coherence between hippocampus and Lob VI was significantly increased relative to other recorded cerebellar regions (Fig. 1*D*, middle; Fig. 3), indicating region-specific cerebello-hippocampal coupling during this sleep state. Furthermore, significant modulation of δ and theta coherence across sleep states was present in HPC-Lob VI and HPC-Lob II/III recording combinations, while remaining stable between HPC-Crus I (Fig. 1*D*, middle; Fig. 3). In contrast, during REM sleep, coherence patterns were similar to wake, with the most prominent peaks observed in the theta and low-frequency range (<1 Hz; Fig. 1*D*, right; Fig. 3). In summary, by characterizing the spectral properties of cerebello-hippocampal network LFP during wake and sleep, we reveal that coherence between these regions is sleep state-dependent and particularly prominent between hippocampus and Lob VI during the non-REM stage of sleep.

REM-associated cerebellar PSPs phase-lock to both local cerebellar and distant hippocampal oscillations, respectively

In addition to the striking sleep state-related changes observed in ongoing cerebellar LFP oscillations, we also noted prominent PSP events (large-amplitude voltage fluctuations of 129.5 ± 5.68 ms duration and 2.31 ± 0.15 *z* score amplitude) across the three cerebellar recording sites (Fig. 4*A–C*). PSPs occurred in all three cerebellar regions at similar times (cross-correlation between all pairs of cerebellar recorded PSPs revealed a peak at 0 latency; Fig. 4*A–C*) and were found during both REM and non-REM epochs; however, they occurred in greatest numbers during REM (Fig. 4*A*,*D*). Moreover, PSPs occurred in concentrated clusters during REM (interevent interval <1 s) but were distributed more sparsely during non-REM (Fig. 4*E*). We also observed that during REM epochs, PSPs tended to occur at specific phases of the ongoing cerebellar δ waves in all three cerebellar regions (Fig. 4*A*). This observation was confirmed by computing the distribution of PSP events relative to the phase of REM-associated cerebellar δ waves (Fig. 4*F–H*; PSPs occurred most often near the peak of the cycle with a preferred angle of 350.6 ± 2.248° and with similar levels across all three cerebellar regions, Fig. 4*G*,*H*). Next, we investigated phase-locking of PSPs recorded in the cerebellum relative to hippocampal LFP theta phase during REM (Fig. 4*I*), which revealed that these events occur consistently near the trough of the theta cycle (preferred phase angle, 147.4 ± 15.93°; Fig. 4*I*) and at similar levels across cerebellar regions (Fig. 4*J*,*K*).

Intracerebellar cross-frequency modulation: cerebellar δ is a modulator of VHFOs during REM

The most prominent, ongoing LFP oscillations observed in the cerebellum during REM sleep were found in the δ (<4 Hz) and VHFO (~250 Hz) frequency ranges, respectively (see Fig. 1). Thus, to investigate any relationship between these two oscillators, we conducted cross-frequency spectral analysis (Fig. 5). This revealed that, during REM, the power of cerebellar VHFOs is significantly modulated by the phase of those in the δ range (Fig. 5*B*,*C*). Interestingly, this modulation was significant only in vermal regions (Lob VI, Lob II/III) and not in Crus I. This finding is consistent with the reduced presence of VHFOs during REM in the Crus I cerebellar region compared with the others recorded (Figs. 1*C*, 2*C*,*D*), further indicating spatial heterogeneity in cerebellar processing during sleep.

Since PSPs were highly abundant during REM and also phase-locked to cerebellar δ, we investigated whether they play a role in local cross-frequency modulation between δ phase and

←

with both slow, phasic, and very high-frequency (~250 Hz) cerebellar oscillations. ***C***, Mean power spectra for each of the defined states (HPC, $n = 20$; Crus I, $n = 11$; Lob VI, $n = 15$; Lob II/III, $n = 11$). ***D***, Mean coherence between HPC-Crus I ($n = 11$), HPC-Lob VI ($n = 15$), and HPC-Lob II/III ($n = 11$) across states. ***E***, Intracerebellar δ coherence is highest during REM sleep. δ band (<4 Hz) coherence was elevated during REM sleep compared with both awake and non-REM in all combinations of cerebellar recordings (Crus I-Lob II/III, $n = 8$; Crus I-Lob VI, $n = 7$; Lob II/III-Lob VI, $n = 7$). Shading represents SEM calculated across animals.

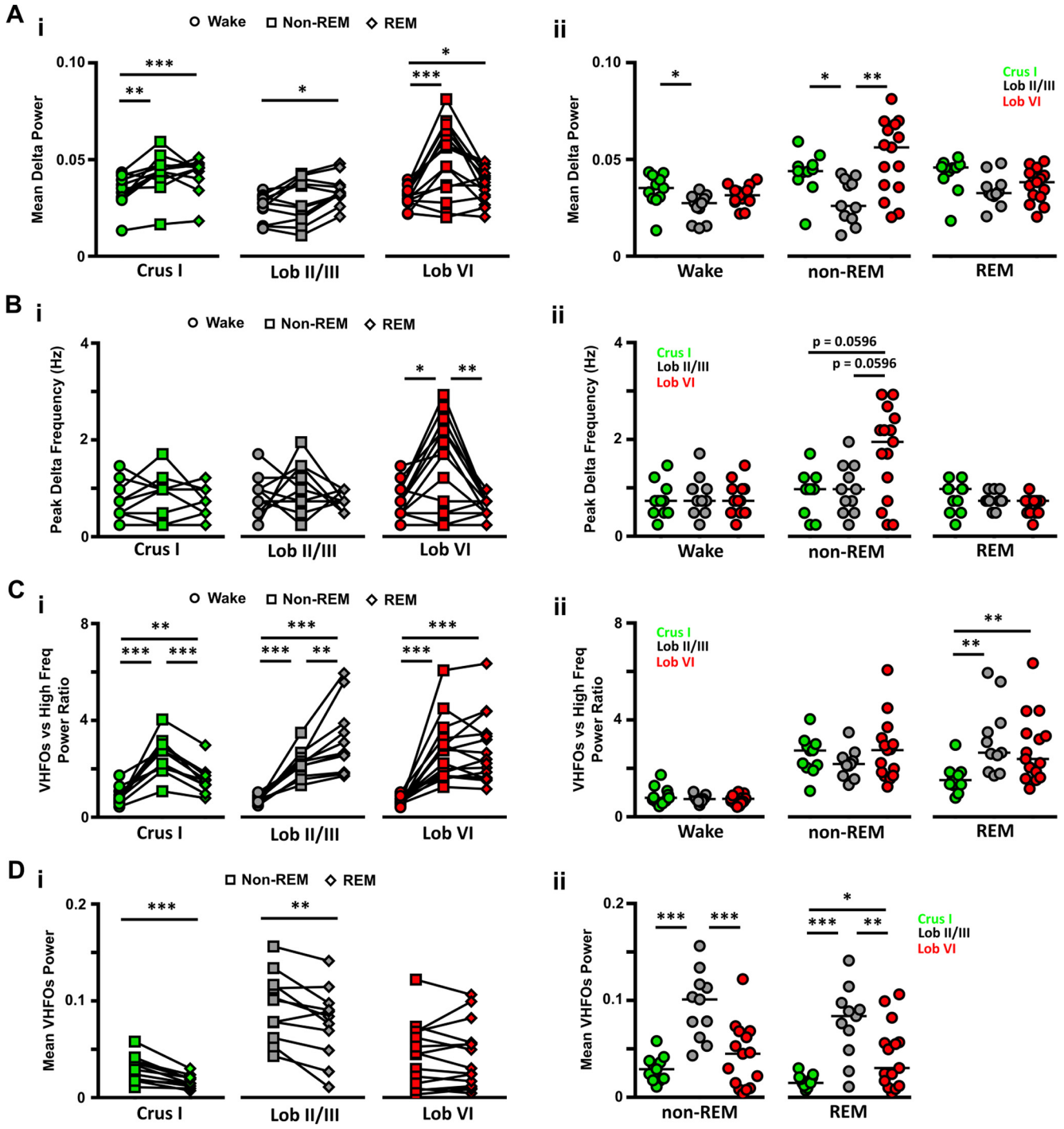

Figure 2. LFP power in δ (0.1-4 Hz) and VHFO (240-280 Hz) frequency bands during wake and sleep. ***Ai***, The power of δ oscillations varied between wake and the different sleep states within the three cerebellar regions. ***Aii***, Similarly, differences between cerebellar regions were observed both during wake. ***Bi***, The peak δ band frequency differed across sleep states only in Lob VI. ***Bii***, Differences in the peak δ frequency band across cerebellar regions were also restricted to non-REM epochs. ***Ci***, During wake, the power of VHFOs was lower compared with high-frequency oscillations in all regions, as indicated by the mean values <1. In contrast, during sleep, across all recorded cerebellar regions, the ratio of VFHO to high-frequency oscillation power increased significantly compared with wake (shifted to values >1), and also differed between sleep states. ***Cii***, Significant differences across cerebellar regions were restricted to REM epochs when Crus I showed significantly smaller ratios than the other two regions. ***Di***, VHFO power was significantly reduced during REM sleep compared with non-REM in Crus I and Lob II/III but remained unchanged in Lob VI. ***Dii***, VHFO power was significantly higher in Lob II during both non-REM and REM sleep. For Crus 1, $n = 11$; Lob VI, $n = 15$; Lob II/III, $n = 11$. For detailed statistical comparisons, see Extended Data Figure 2-1. $^{*}p < 0.05$. $^{**}p < 0.01$. $^{***}p < 0.001$.

VHFO power. By comparing modulation in δ cycles with no PSPs, those containing isolated PSPs and those containing clusters of PSPs (Fig. 5*D*), we found that PSP density did not significantly influence the degree of cross-frequency modulation observed in any of the recorded cerebellar regions (Fig. 5*D*).

Cerebellar δ and phasic sharp potentials modulate hippocampal theta oscillations during REM

We next investigated whether the prominent cerebellar δ oscillations and the high density of PSPs observed during REM were related to, or impacted on, theta oscillations in the hippocampus,

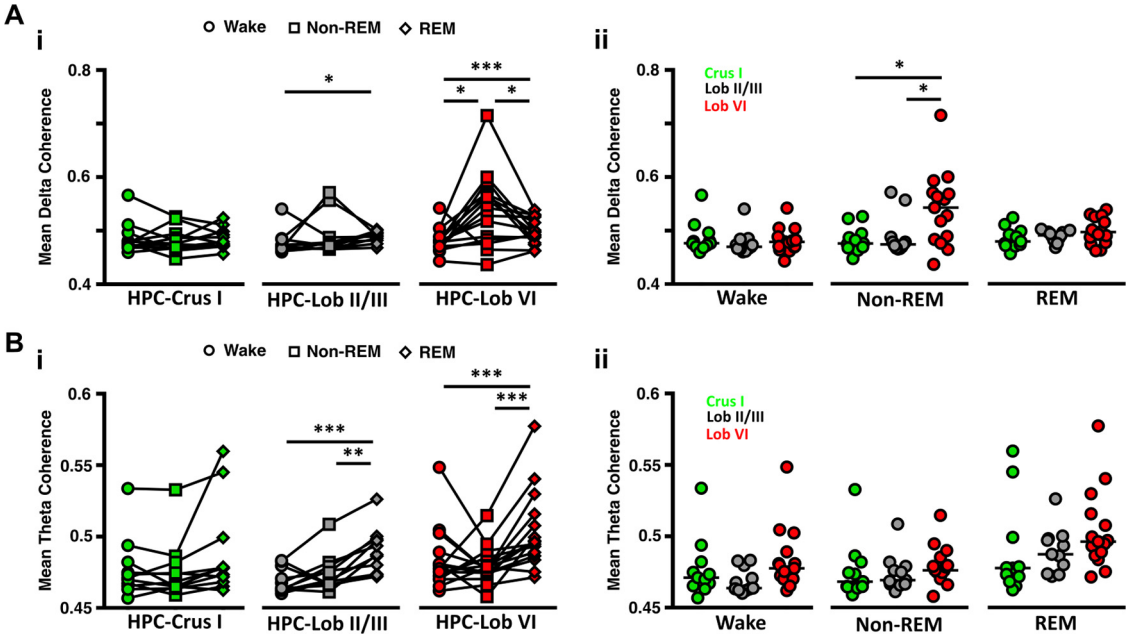

Figure 3. Cerebello-hippocampal coherence in the δ (<4 Hz) and theta (6-12 Hz) frequency ranges is modulated across sleep states. ***Ai***, Significant modulation across sleep states in δ coherence was found between hippocampus and Lob II/III and particularly between the hippocampus and Lob VI. Hippocampus-Crus I δ coherence remained unchanged ($n = 11$, Friedman test, $p = 0.8438$). ***Aii***, Significant differences in δ coherence between the cerebello-hippocampal combinations were restricted to non-REM epochs, with HPC-Lob VI levels being significantly higher than other combinations. ***Bi***, Similarly, theta coherence was significantly increased during REM sleep between HPC-Lob II/III, but remained stable across sleep states between the HPC-Crus. ***Bii***, In contrast, no differences across cerebello-hipocampal combinations were found during any of the states analyzed. For Crus 1, $n = 11$; Lob VI, $n = 15$; Lob II/III, $n = 11$. For detailed statistical comparisons, see Extended Data Figure 2-1. $^*p < 0.05$. $^{**}p < 0.01$. $^{***}p < 0.001$.

which are a well-described physiological signature of REM sleep (Fig. 6). During REM, hippocampal theta oscillations fluctuated within a frequency range of ~6-12 Hz, and visual inspection of spectra and raw LFP traces revealed that these theta frequency fluctuations appeared to be temporally aligned with cerebellar δ oscillation cycles/PSP events (Fig. 6*A*). Therefore, we next calculated hippocampal LFP power spectra triggered from the peak of cerebellar δ wave cycles. This analysis revealed that hippocampal theta frequency increased during the ascending phase of the cerebellar δ oscillation compared with the values at the trough ($-\pi$; Fig. 6*B*,*C*).

Given that PSP timing is locked to specific phases of both cerebellar δ and hippocampal theta oscillation cycles (Fig. 4), we next investigated whether the number of PSPs occurring during the cerebellar δ wave was associated with the level of hippocampal theta modulation. In contrast to intracerebellar δ phase modulation of VHFOs, by comparing cycles with no PSPs, those containing isolated PSPs and those containing clusters of PSPs (Fig. 6*D*), we found that the acceleration of hippocampal theta was most prominent when clusters of cerebellar PSPs were present, suggesting that these phasic events are linked to the observed changes in hippocampal theta frequency.

Hippocampal ripples drive LFP changes in the cerebellum

During REM, dominant hippocampal theta oscillations are coordinated with prominent cerebellar LFP network activity (δ oscillations and PSPs). During non-REM sleep, however, hippocampal activity is characterized by the presence of prominent SWRs. Therefore, we next asked whether cerebellar activity is coordinated or modulated by hippocampal SWRs during non-REM sleep. To address this question, we first detected SWRs (Fig. 7*A*) and computed the cerebellar LFP averaged relative to SWR onset (Fig. 7*B*). ERPs were clearly observed in all the recorded cerebellar regions. The SWR-triggered responses were characterized by a prominent slow component that preceded the onset timing of SWR maximal amplitude followed by an ERP (occurring after SWR ripple maximal amplitude; Fig. 7*B*). In order to isolate the ERPs from the slow component and compare their amplitude across cerebellar regions, we baselined them by subtracting the pre-SWR levels (mean values from −100 to −50 ms; Fig. 7*B*, inset). The onset-to-peak amplitude in baselined ERPs did not differ across cerebellar regions (Fig. 7*C*, left). In contrast, latency to ERP onset was shortest in Lob VI (11.13 ± 3.93 ms) compared with Crus I (28.91 ± 4.72 ms) and to Lob II/III (32.18 ± 3.85 ms; Fig. 7*C*, right). Given the recent description of SWR propagation from hippocampus to neocortex (Nitzan et al., 2020), we also calculated SWR-triggered spectral analysis of the cerebellar LFP (Fig. 7*D*,*E*), which revealed no significant changes in cerebellar LFP power in 140-180 Hz range (SWR frequency range). This suggests that hippocampal SWRs do not propagate directly or indirectly to the cerebellum. We next asked whether the slow-frequency component observed in the SWR-triggered responses resulted from the timing of SWRs at the peak of cerebellar slow oscillation cycles. To probe this question, we calculated phase-locking of the detected hippocampal SWR relative to the phase of cerebellar δ oscillations (<4 Hz; Fig. 7*F*–*H*). We confirmed that hippocampal SWRs were phase-locked to the δ rhythm observed in all three recorded cerebellar regions but that the strength of phase-locking was significantly greatest for Lob VI (Fig. 7*G*,*H*). Finally, we investigated potential interplay between PSPs recorded in the cerebellum and hippocampal SWRs. To do so, we computed the probability of detecting a SWR following the detection of a PSP. We found a consistent decrease in SWR probability ~90 ms after the PSP peak in all cerebellar regions, which lasted for ~1 s (compared with a shuffled dataset; Fig. 7*I*). In addition, a significant increase in SWR was observed ~100 ms before the PSPs recorded in Lob VI. The reduction in SWR occurrence immediately following the PSPs suggests

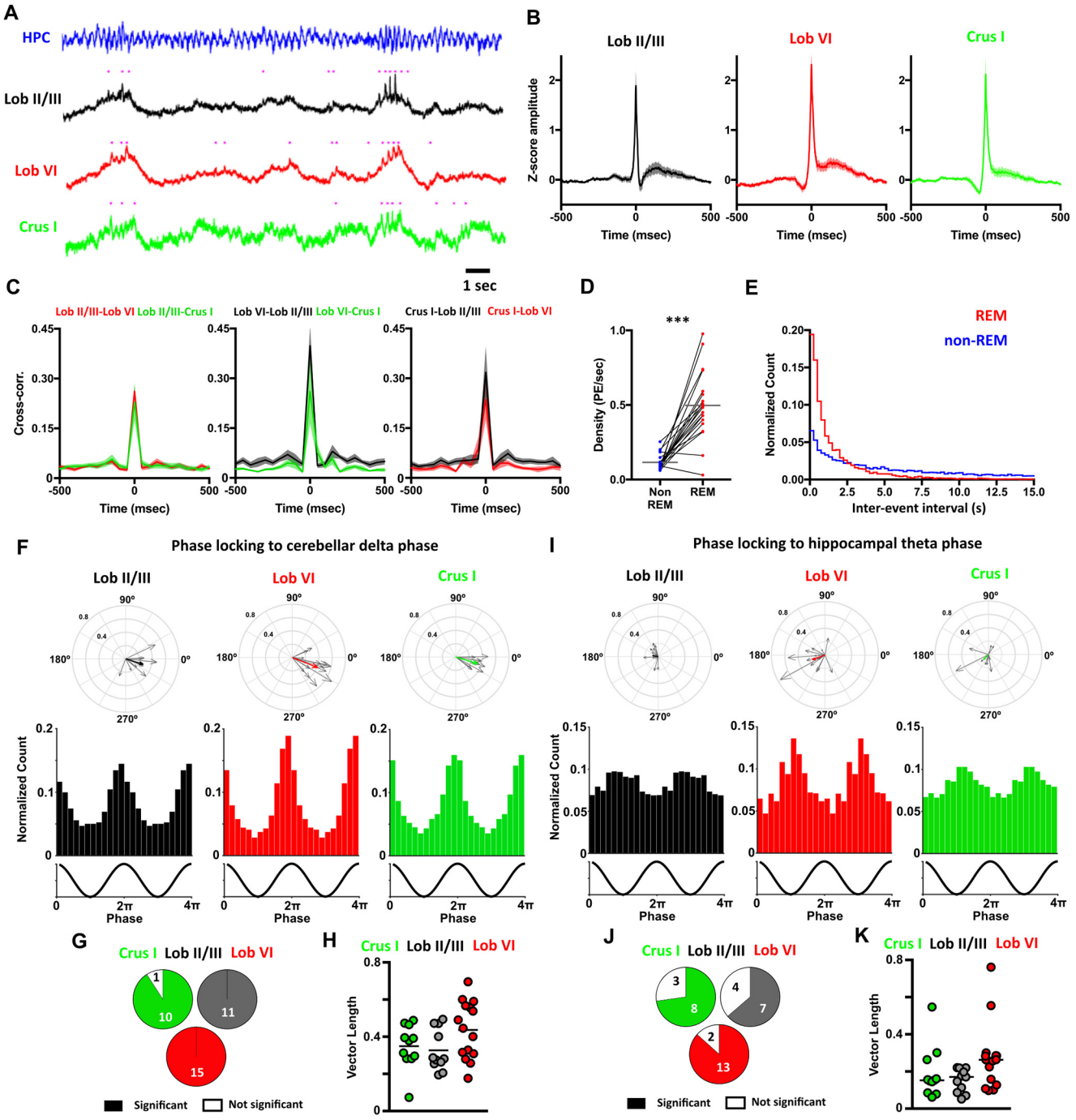

Figure 4. Phasic potentials (PSPs) occur at preferred phases of cerebellar δ and hippocampal theta oscillations during REM. ***A***, We observed PSPs in the cerebellar LFP recordings during REM (indicated by purple dots), which occurred preferentially during up phase of the δ oscillations. Moreover, hippocampal theta frequency was transiently accelerated during the up phase of the cerebellar δ oscillations. ***B***, PSPs were found in all cerebellar recording sites and all mice. Averaged waveforms across animals (Lob II/III, $n = 11$; Lob VI, $n = 15$; Crus I, $n = 11$). ***C***, Cross-correlograms between the PSPs detected at a given cerebellar region and those recorded in the others. All cross-correlograms show a peak with $\leq$50 ms lag, suggesting that most of the PSPs co-occurred at the three cerebellar regions near simultaneously. ***D***, PSPs were observed during non-REM and REM sleep; however, the density of these events was significantly higher during REM (non-REM density = 0.1152 $\pm$ 0.012 PSPs/s; REM density = 0.4973 $\pm$ 0.050 PSPs/s; Wilcoxon test, $p < 0.0001$). ***E***, The distributions of the interevent intervals (IEIs) were significantly different between non-REM and REM epochs (two-sample Kolmogorov–Smirnov test, $p < 0.0001$). During REM, PSPs were preferentially concentrated as clusters (IEIs < 1 s). ***F***, PSPs recorded at all cerebellar regions were phase-locked to the local δ oscillations during REM. Top panels, The individual vectors of the phase-locking for each mouse (gray arrows) and the average vector across all mice (color-coded; resultant vector angle: Crus I = 342.97°, Lob II = 343.05°, Lob VI = 338.67°; resultant vector length: Crus I = 0.34, Lob II = 0.28, Lob VI = 0.41). Bottom panels, The normalized count of PSPs recorded at the different phases of δ oscillations in all mice for each cerebellar region. ***G***, Fraction of mice with significant phase-locking (significant phase-locking was found in Crus I, 10/11 mice; Lob II/III, 11/11 mice; Lob VI 15/15 mice). ***H***, The level of the phase-locking did not differ across cerebellar regions (one-way ANOVA, $p = 0.0932$). ***I-K***, Same as for ***F-H***, but here calculating phase-locking of PSPs detected in the cerebellum to ongoing hippocampal theta oscillations. ***I***, Top row, Lob II/III Rayleigh's test, $p < 0.001$; Lob VI Rayleigh's test, $p < 0.001$; Crus I Rayleigh's test, $p < 0.001$. ***J***, Fraction of mice with significant phase-locking of PSPS to hippocampal theta (significant phase-locking was found in Crus I, 8/11 mice; Lob II/III, 7/11 mice; Lob VI 13/15 mice). ***K***, The level of the phase-locking to hippocampal theta did not differ across cerebellar regions. For detailed statistical comparisons, see Extended Data Figure 2-1. ***$p < 0.001$.

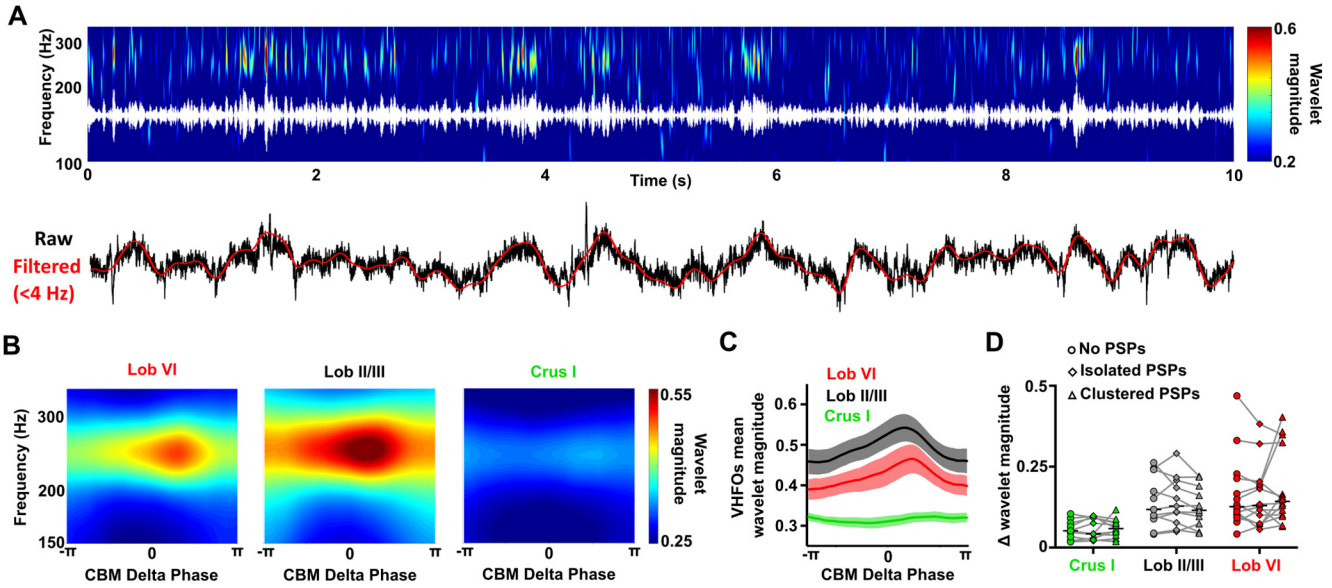

Figure 5. Modulation of VHFO frequency oscillations by δ oscillations within the cerebellum during REM. ***A***, Representative spectrogram (top; with VHFO frequency filtered trace overlaid in white) and raw cerebellar LFP recordings (bottom; with δ frequency filtered oscillations overlaid in red) showing the modulation of VHFOs by cerebellar δ oscillations during an REM epoch. The cerebellar LFP is dominated by both δ oscillations and VHFOs, which fluctuate dynamically within the ~250 Hz and <4 Hz ranges, respectively. The fluctuations in cerebellar VHFO power appear temporally aligned to the prominent δ oscillations in the cerebellar LFP. ***B***, Average spectrograms aligned to the phase of the cerebellar (CBM) δ oscillations (<4 Hz) during REM sleep. The power of cerebellar VHFOs appears greatest following the peak of cerebellar δ (zero phase radians) in vermal lobules (VI, II/III) but not Crus I. ***C***, Average cerebellar VHFO power aligned to cerebellar δ oscillation phase. A significant increase in VHFO power was found across δ phase in Lob VI and Lob II/III. ***D***, Effect of PSP abundance during the cerebellar δ oscillations on the modulation of VHFOs during REM. We compared the maximal change in cerebellar VHFO power during cerebellar δ oscillations in which no PSPs, isolated PSPs or clusters of PSPs were detected. No significant differences were observed for the three cerebellar regions. In all mean plots, n = Lob VI, $n = 15$ mice; Crus I, $n = 11$ mice; Lob II/III, $n = 11$ mice. For detailed statistical comparisons, see Extended Data Figure 2-1.

that the latter have an impact on local hippocampal activity, while the higher probability preceding the PSPs suggests a potential association between the occurrence of SWR and the generation of PSPs.

Discussion

Despite the extensive literature on sleep-related neurophysiological processes in the hippocampus (Klinzing et al., 2019) and recent advances in understanding of sleep-related processes in the cerebellum (Canto et al., 2017; Xu et al., 2020; Zhang et al., 2020), no report exists on potential functional or physiological interplay between these regions during sleep. Therefore, to bridge this knowledge gap, we investigated cerebello-hippocampal interactions as well as intrinsic cerebellar LFP dynamics across sleep states in mice.

Intracerebellar LFP dynamics during sleep

We profiled sleep-related activity within three distinct regions of the cerebellar cortex: Lob VI, Lob II/III, and Crus I. Modulation of cerebellar LFP activity was found across sleep states, both locally, in spatially segregated cerebellar lobules, and globally, in a coordinated manner across the cerebellar cortex. Overall, during REM and non-REM sleep, prominent δ oscillations (<4 Hz) and VHFOs (~250 Hz) dominate the spectral profile in all three regions. The presence of VHFOs has been described previously in Lob V/VIa of anesthetized and awake, head-fixed rats, and attributed to activity in recurrent Purkinje cell collaterals (de Solages et al., 2008). In contrast, previous studies in freely moving mice have predominantly described high-frequency oscillations in the cerebellar cortex (~150 Hz) (Cheron et al., 2004, 2005; Servais et al., 2005), which is consistent with our observations during wake. Thus, given the high presence of VHFOs in head-fixed or sleeping animals, they may be related to the absence of voluntary movements. Our findings additionally extend the work of de Solages et al. (2008) by showing, for the first time, that VHFOs are concurrently present across multiple cerebellar cortical regions, prevalent during sleep (above wake levels), and temporally coordinated by local cerebellar δ rhythms during REM sleep. Despite these advances, further work is clearly required to fully understand the functional importance of VHFOs in the cerebellum (De Zeeuw et al., 2008).

During non-REM sleep, our description of prominent δ oscillations in the cerebellar cortex is in keeping with previous work showing that neocortical slow oscillations entrain those in the cerebellar cortex (Roš et al., 2009; Rowland et al., 2010; Xu et al., 2020). In contrast, REM sleep is traditionally associated with theta (~6-12 Hz) frequency LFP oscillations. Our recordings from the cerebellum revealed no increase in theta power during REM. Surprisingly, we did observe highly synchronous δ (<4 Hz) oscillations in all three recorded cerebellar regions during REM. This may be a local circuit peculiarity; however, recent evidence in rodent and human studies suggests that localized δ oscillations should be considered an integral component of REM sleep (Funk et al., 2016; Siclari and Tononi, 2017; Bernardi et al., 2019).

Cerebello-hippocampal coherence during sleep

Next, we sought evidence for putative functional coupling, as measured by LFP-LFP coherence, between the hippocampus and cerebellum across sleep states. Of particular note, we found that hippocampus-Lob VI coherence was significantly and dynamically

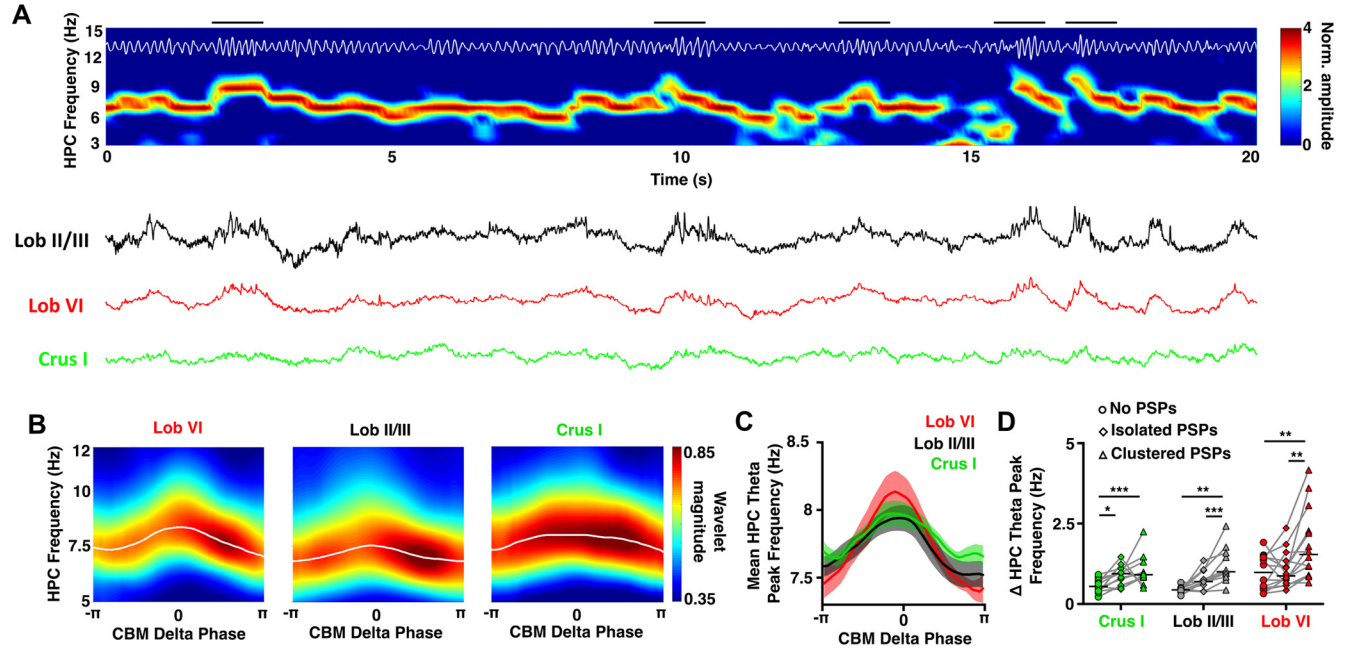

Figure 6. Modulation of hippocampal theta frequency by cerebellar (CBM) δ oscillations during REM. ***A***, Representative spectrogram (top; with theta filtered trace overlaid in white) and raw cerebellar LFP recordings (bottom) showing the modulation of hippocampal theta frequency by cerebellar δ oscillations during an REM epoch. The hippocampal LFP is dominated by theta oscillations, which fluctuate dynamically within the 6-12 Hz range. These fluctuations in hippocampal theta frequency appear temporally aligned to the δ oscillations dominating cerebellar LFPs (examples of this are indicated by black horizontal bars above spectrogram). ***B***, Average hippocampal spectrograms aligned to the phase of the cerebellar δ oscillations (<4 Hz) during REM sleep. The preferred hippocampal theta frequency (white line, overlaid) shows an acceleration coincident with the peak of the cerebellar δ oscillations: 0 phase radians; maximal frequency of hippocampal theta: triggered from Crus I = 7.97 ± 0.095 Hz at −18.74° (−0.1 π), triggered from Lob II/III = 7.94 ± 0.095 Hz at −3.72° (−0.02 π), triggered from Lob VI = 8.14 ± 0.154 Hz at −18.74° (−0.1 π). ***C***, Average preferred hippocampal theta frequency aligned to cerebellar δ oscillation phase. Significant hippocampal theta frequency acceleration was found from the trough of δ to the peak of δ in all cerebellar regions. However, no differences in hippocampal theta frequency modulation were observed between the δ oscillations recorded across the three cerebellar locations. ***D***, Effect of PSP abundance during the cerebellar δ oscillations on the modulation of preferred hippocampal theta frequency during REM. We compared the maximal change in hippocampal theta frequency during cerebellar δ oscillations in which no PSPs, isolated PSPs, or clusters of PSPs were detected. Significant differences were observed for the three cerebellar regions with a significant increase in the hippocampal theta modulation during δ waves when clusters of PSPs were detected compared with those with no PSPs or isolated PSPs. In all mean plots, n = Lob VI, n = 15 mice; Crus I, n = 11 mice; Lob II/III, n = 11 mice. For detailed statistical comparisons, see Extended Data Figure 2-1. *p < 0.05. **p < 0.01. ***p < 0.001.

modulated across sleep states. Specifically, during non-REM, hippocampus-Lob VI δ coherence was significantly higher than during wake/REM, whereas during REM, hippocampus-Lob VI theta coherence was significantly higher than during non-REM and, surprisingly, was also significantly modulated to above wake levels. The comparatively heightened, frequency-specific, offline coupling between hippocampus and Lob VI during non-REM illustrates the potential for both sleep stage and regionally specific interactions between the two brain structures in addition to those we previously described during active movement in the home-cage (Watson et al., 2019). This interaction may be supported by anatomic connections linking Lob VI and hippocampus via the medial septum or the supramammillary nucleus (Watson et al., 2019).

Putative PGO waves provide a potential substrate for cerebello-hippocampal interactions during REM

In addition to the ongoing LFP oscillations observed in the cerebello-hippocampal network during sleep, we also detected high-amplitude PSPs in the cerebellar cortical recordings that were particularly abundant during REM sleep. Previous studies have described similar phasic events in the cerebellum and attributed them to propagation of PGO waves (Farber et al., 1980; Velluti et al., 1985). In keeping with our observations, PGO waves are found to be highly concentrated in REM epochs across multiple brain regions (Harlay et al., 1974; Pellet and Harley, 1977; Marks et al., 1980; Tsunematsu et al., 2020). Furthermore, PGO waves are known to phase-lock to hippocampal theta rhythms during REM and modulate its frequency (increasing the preferred theta frequency) (Karashima et al., 2002, 2007). We also show that cerebellar PSPs are significantly phase-locked to the cerebellar δ oscillation cycle, and cross-frequency analysis revealed that cerebellar δ modulation of hippocampal theta oscillations occurs preferentially when PSP content is high. Overall, the most parsimonious explanation is that the PSPs we recorded in the cerebellum are propagated PGO waves. During REM, PGOs have been shown to play a crucial role in coordinating long range network dynamics underlying sleep-dependent cognitive processes required for establishment of fear memory (Datta et al., 1998; Datta, 2000; Datta and O'Malley, 2013). The PSPs observed in the cerebellum may play a similar role by coordinating interactions with the hippocampus.

SWRs link hippocampus and cerebellum during non-REM sleep

SWRs are a prominent physiological feature of hippocampal activity during non-REM sleep (Buzsáki, 1986; Csicsvari et al., 2000). Their occurrence is coordinated with cortical spindles, which are themselves synchronized with cortical slow-δ oscillations (Siapas and Wilson, 1998), and this tripartite interaction is important for memory formation (Girardeau et al., 2009; Maingret et al., 2016; Latchoumane et al., 2017). Consequently, we examined the relationship between hippocampal SWRs and cerebellar LFPs. SWR-triggered cerebellar LFP waveform averages in combination with phase-locking analysis revealed two main findings. First, ERPs are present in the cerebellar LFP at

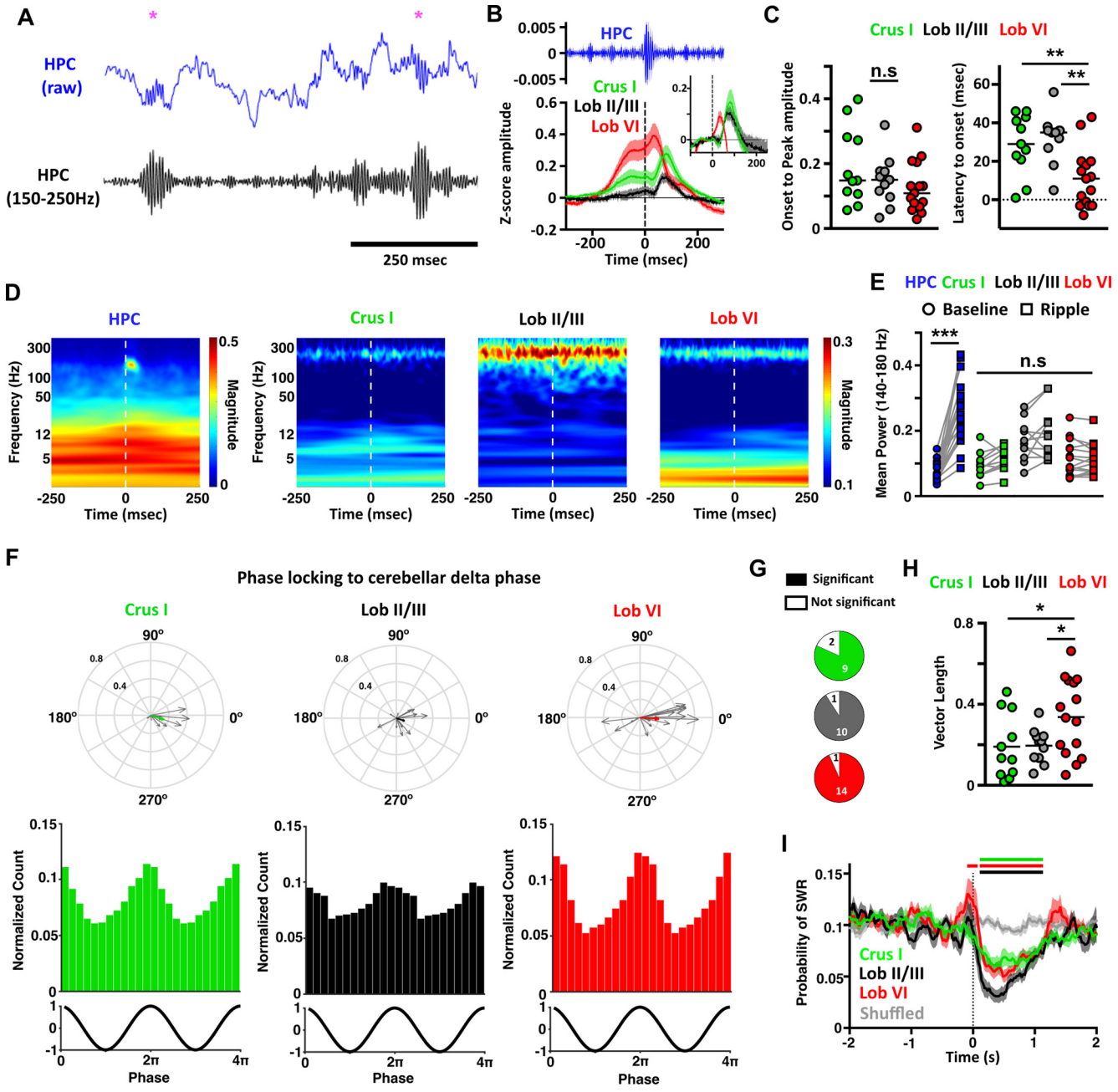

Figure 7. Hippocampal SWRs trigger evoked activity in the cerebellum, and cerebellar PSP events reduce probability of hippocampal SWR occurrence. ***A***, Example of the raw (blue) and filtered (150-250 Hz, black) hippocampal LFP during non-REM sleep. SWRs were identified (purple asterisks) at the maximal value in the filtered signal. ***B***, Averaged SWR-triggered waveforms from the cerebellar recordings. Zero time represents the time of detected SWR onset in the filtered signal. Evoked field potentials were observed in all the cerebellar recordings. Inset, The same data but baselined against values from −100 to −50 ms, eliminating the slow-frequency component and allowing clearer visualization of the evoked potentials. ***C***, From the baseline normalized data, we quantified the ERP amplitude measured as the onset-to-peak value and also the onset latency. No significant differences were observed for amplitude; however, Lob VI ERPs occurred at significantly shorter latencies compared with both Lob II/III and Crus I. ***D***, Averaged power spectra triggered by detected hippocampal SWR events (time 0). We observe discrete SWR activity in the hippocampal spectrogram (~150 Hz) that is not present in the cerebellum. ***E***, Mean spectral power in the 140-180 Hz range calculated in windows of 250 ms pre- and post-detected SWR onset. Significant increases in this frequency range were only detected in hippocampal signals. ***F***, Significant phase-locking of SWRs to δ oscillations was found in all cerebellar regions during non-REM sleep. Bottom panels, The normalized count of PSPs recorded at the different phases of δ oscillations in all mice for each cerebellar region. Top, The individual vectors of the phase-locking for each mouse (gray arrows) and the average vector across all mice (color-coded; resultant vector angle: Crus I = 341.53°, Lob II = 342.10°, Lob VI = 355.27°; resultant vector length: Crus I = 0.16, Lob II = 0.1, Lob VI = 0.21). ***G***, Fraction of mice with significant SWR-to-cerebellar δ phase-locking (significant phase-locking was found in Crus I, 9/11 mice; Lob II/III, 10/11 mice; Lob VI 14/15 mice). ***H***, The level of SWR phase-locking was higher with Lob VI compared with Crus I or Lob II/III. ***I***, Probability of SWRs relative to PSP onset. The number of SWRs are reduced following PSP occurrence. Color bars represent significant differences in PSP probability relative to shuffled data (Lob VI, red; Crus I, green; Lob II/III, black; two-way ANOVA with multiple comparisons between cerebellar region and shuffled data). For all mean plots, HPC, $n = 20$ mice; Crus 1, $n = 11$ mice; Lob II/III, $n = 11$ mice; Lob VI, $n = 15$ mice. For detailed statistical comparisons, see Extended Data Figure 2-1. $^*p < 0.05$. $^{**}p < 0.01$. $^{***}p < 0.001$.

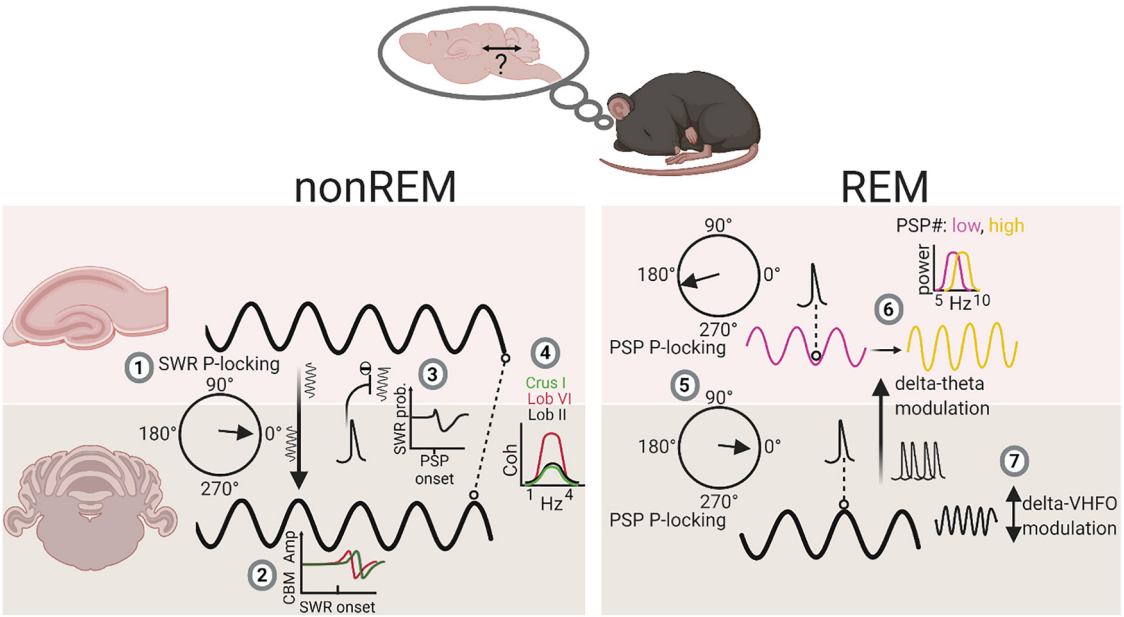

Figure 8. Summary diagram of main findings illustrating sleep stage-specific physiological events and interactions within the cerebello-hippocampal network. During non-REM, hippocampal SWRs are phase-locked to the cerebellar δ oscillation (1) and drive modulation of cerebellar LFP activity, at shortest latency in Lob VI (2). In addition, PSPs recorded in the cerebellum are associated with reduced SWR probability of occurrence. Finally, overall coherence within the δ frequency range is highest between hippocampus and Lob VI compared with other cerebellar lobules. During REM, PSPs are significantly phase-locked to both the trough of hippocampal theta (purple line) and the peak of cerebellar δ oscillations (black line) (5). Cerebellar δ oscillations and associated PSPs modulate the frequency of hippocampal theta rhythms (from ~7.5 Hz [low, purple line] to 8 Hz [high, yellow line]) (6). Additionally, within the cerebellum, δ oscillations can modulate activity within the VHFO range during REM (7). P-locking, phase-locking. The multisite LFP recording technique used in our study allowed us to survey a large spatial extent of the cerebellum (hemispheric, Crus I; dorsal vermis, Lob VI; and ventral vermis, Lob II/III) alongside hippocampal LFP, which would be difficult to achieve using alternative methods. However, this methodology precluded layer-specific or local spiking activity measurement. Future studies directly measuring spiking activity across both regions during sleep will be essential to fully understand the functional significance of the dynamics observed at the LFP level. Created with www.BioRender.com.

short latency (particularly in Lob VI) following hippocampal SWR onset. Previously, hippocampal SWRs have been shown to drive evoked LFP and single-unit changes in the cingulate cortex of a similar latency to those triggered by hippocampal electrical stimulation; as such, SWR activity may be considered indicative of hippocampal efference (Wang and Ikemoto, 2016). Indeed, we found that SWRs triggered cerebellar ERPs with a short onset latency of ~10 ms, which is in agreement with previous reports in anesthetized rats (Saint-Cyr and Woodward, 1980a, b) where electrical stimulation of the hippocampal fornix elicited both short-latency mossy fiber (5-10 ms, routed via the pontine nuclei) and longer-latency, climbing fiber (10-20 ms, routed via the inferior olive) responses within the cerebellar cortex. Also consistent with our results, topographical mapping of cerebellar responses following hippocampal electrical stimulation revealed evoked activity mainly in the Lob VI region of both cats (Newman and Reza, 1979) and rats (Saint-Cyr and Woodward, 1980a).

Our second main finding was that SWRs are significantly phase-locked to the up state of cerebellar δ oscillations in striking similarity to the well-described locking of SWRs to neocortical δ, which is thought to facilitate transfer of memory information from subcortical to cortical loci (Maingret et al., 2016). As cerebellar Purkinje cells are known to toggle between depolarizing "up states" and hyperpolarizing "down states" (for review, see Engbers et al., 2013), it may be considered that, during non-REM sleep, cerebellar δ oscillations facilitate the transfer of hippocampal information via phase-locking of SWRs to periods of high Purkinje cell excitability. Consistent with our finding that hippocampus-Lob VI δ coherence during non-REM sleep is higher compared with other cerebellar regions, SWRs were significantly more phase-locked to Lob VI δ compared with Crus I or Lob II/III. Another physiological explanation of SWR links to cerebellar δ oscillations may be provided by the fact that SWRs are known to nest in the up state of neocortical slow-δ oscillations. In turn, these neocortical oscillations have been shown to entrain cerebellar activity in both anesthetized rats (Roš et al., 2009; Rowland et al., 2010; Schwarz, 2010) and naturally sleeping monkeys (Xu et al., 2020). Thus, SWR phase-locking to cerebellar δ oscillations may be mediated via upstream SWR-to-neocortical δ nesting. Together, the SWR-triggered evoked LFP activity recorded in the cerebellar cortex and their coordination with cerebellar δ oscillations illustrate the existence of robust physiological links and candidate mechanisms that could subserve hippocampal-cerebellar (particularly Lob VI) interactions during non-REM sleep.

Interplay between putative PGOs recorded in the cerebellum and SWRs

Using cross-correlation analysis to investigate interplay between PSPs (putative PGOs) and SWRs, we found a significantly increased probability of SWR occurrence preceding (~100 ms) the occurrence of PSPs, specifically in Lob VI, which aligns with recent findings (Tsunematsu et al., 2020). Following cerebellar PSP onset, the probability of SWR occurrence was reduced for ~1 s, suggesting that these events drive hippocampal circuit changes that temporarily preclude SWR generation and may afford distinct cerebello-hippocampal communication states. Interestingly, this reduction was not observed by Tsunematsu et

al. (2020). However, another recent study in macaque (Ramirez-Villegas et al., 2021) identified two types of PGOs, with differential association with hippocampal events. Of particular relevance, one PGO type was associated with hippocampal theta bursts and a reduced occurrence of SWR. Therefore, it is likely that the identified cerebellar PSPs preferentially represent the occurrence of this specific type of PGOs wave.

In conclusion, our findings illustrate the presence of multiple, bidirectional, and coordinated physiological events in the cerebello-hippocampal network during sleep (see Fig. 8), centered around prominent δ oscillations. In particular, we have highlighted lobule-specific hippocampus-to-cerebellum directed interaction during non-REM sleep mediated via SWR and δ oscillations. During REM, we identified prominent cerebellar δ oscillations and associated PSPs, which modulate both local cerebellar VHFOs and distant hippocampal theta oscillations. Thus, it appears that δ oscillations play a key role in temporal coordination both within and between these regions. Similar sleep stage-specific, transient physiological events have been shown to be important for memory formation across other brain circuits, and it may be hypothesized that the events described in the hippocampal-cerebellar network serve a similar role in affording the two regions the ability to preferentially interact during windows of enhanced synaptic plasticity.

References

Babayan BM, Watilliaux A, Viejo G, Paradis AL, Girard B, Rondi-Reig L (2017) A hippocampo-cerebellar centred network for the learning and execution of sequence-based navigation. Sci Rep 7:17812.

Bernardi G, Betta M, Ricciardi E, Pietrini P, Tononi G, Siclari F (2019) Regional delta waves in human rapid eye movement sleep. J Neurosci 39:2686–2697.

Braun A (1997) Regional cerebral blood flow throughout the sleep-wake cycle: an H2(15)O PET study. Brain 120:1173–1197.

Burguière E, Arleo A, Hojjati M, Elgersma Y, Zeeuw CI, De Berthoz A, Rondi-Reig L (2005) Spatial navigation impairment in mice lacking cerebellar LTD: a motor adaptation deficit? Nat Neurosci 8:1292–1294.

Buzsáki G (1986) Hippocampal sharp waves: their origin and significance. Brain Res 398:242–252.

Canto CB, Onuki Y, Bruinsma B, van der Werf YD, De Zeeuw CI (2017) The sleeping cerebellum. Trends Neurosci 40:309–323.

Cheron G, Gall D, Servais L, Dan B, Maex R, Schiffmann SN (2004) Inactivation of calcium-binding protein genes induces 160 Hz oscillations in the cerebellar cortex of alert mice. J Neurosci 24:434–441.

Cheron G, Servais L, Wagstaff J, Dan B (2005) Fast cerebellar oscillation associated with ataxia in a mouse model of Angelman syndrome. Neuroscience 130:631–637.

Csicsvari J, Hirase H, Mamiya A, Buzsáki G (2000) Ensemble patterns of hippocampal CA3-CA1 neurons during sharp wave-associated population events. Neuron 28:585–594.

Datta S (2000) Avoidance task training potentiates phasic pontine-wave density in the rat: a mechanism for sleep-dependent plasticity. J Neurosci 20:8607–8613.

Datta S, O'Malley MW (2013) Fear extinction memory consolidation requires potentiation of pontine-wave activity during REM sleep. J Neurosci 33:4561–4569.

Datta S, Siwek DF, Patterson EH, Cipolloni PB (1998) Localization of pontine PGO wave generation sites and their anatomical projections in the rat. Synapse 30:409–423.

de Lavilléon G, Lacroix MM, Rondi-Reig L, Benchenane K (2015) Explicit memory creation during sleep demonstrates a causal role of place cells in navigation. Nat Neurosci 18:493–495.

de Solages C, Szapiro G, Brunel N, Hakim V, Isope P, Buisseret P, Rousseau C, Barbour B, Léna C (2008) High-frequency organization and synchrony of activity in the Purkinje cell layer of the cerebellum. Neuron 58:775–788.

De Zeeuw CI, Hoebeek FE, Schonewille M (2008) Causes and consequences of oscillations in the cerebellar cortex. Neuron 58:655–658.

Diekelmann S, Born J (2010) The memory function of sleep. Nat Rev Neurosci 11:114–126.

Engbers JD, Fernandez FR, Turner RW (2013) Bistability in Purkinje neurons: ups and downs in cerebellar research. Neural Netw 47:18–31.

Farber J, Marks GA, Roffwarg HP (1980) Rapid eye movement sleep PGO-type waves are present in the dorsal pons of the albino rat. Science 209:615–617.

Franklin K, Paxinos G (2007) The mouse brain in stereotaxic coordinates, Ed 3. Amsterdam: Elsevier.

Funk CM, Honjoh S, Rodriguez A, Cirelli C, Tononi G (2016) Local slow waves in superficial layers of primary cortical areas during REM sleep. Curr Biol 26:396–403.

Geva-Sagiv M, Nir Y (2019) Local sleep oscillations: implications for memory consolidation. Front Neurosci 13:813.

Girardeau G, Benchenane K, Wiener SI, Buzsáki G, Zugaro MB (2009) Selective suppression of hippocampal ripples impairs spatial memory. Nat Neurosci 12:1222–1223.

Harlay F, Pellet J, Tardy MF, Dubrocard S (1974) Activité unitaire corticocérébelleuse et mouvements oculaires: modifications associées aux saccades du sommeil et de la veille. Physiol Behav 12:939–949.

Hobson JA, McCarley RW (1972) Spontaneous discharge rates of cat cerebellar Purkinje cells in sleep and waking. Electroencephalogr Clin Neurophysiol 33:457–469.

Jahnke K, von Wegner F, Morzelewski A, Borisov S, Maischein M, Steinmetz H, Laufs H (2012) To wake or not to wake? The two-sided nature of the human K-complex. Neuroimage 59:1631–1638.

Karashima A, Nakamura K, Sato N, Nakao M, Katayama N, Yamamoto M (2002) Phase-locking of spontaneous and elicited ponto-geniculo-occipital waves is associated with acceleration of hippocampal theta waves during rapid eye movement sleep in cats. Brain Res 958:347–358.

Karashima A, Katayama N, Nakao M (2007) Phase-locking of spontaneous and tone-elicited pontine waves to hippocampal theta waves during REM sleep in rats. Brain Res 1182:73–81.

Kaufmann C, Wehrle R, Wetter TC, Holsboer F, Auer DP, Pollmächer T, Czisch M (2006) Brain activation and hypothalamic functional connectivity during human non-rapid eye movement sleep: an EEG/fMRI study. Brain 129:655–667.

Klinzing JG, Niethard N, Born J (2019) Mechanisms of systems memory consolidation during sleep. Nat Neurosci 22:1598–1610.

Latchoumane CF, Ngo HV, Born J, Shin HS (2017) Thalamic spindles promote memory formation during sleep through triple phase-locking of cortical, thalamic, and hippocampal rhythms. Neuron 95:424–435.e6.

Lefort JM, Vincent J, Tallot L, Jarlier F, De Zeeuw CI, Rondi-Reig L, Rochefort C (2019) Impaired cerebellar Purkinje cell potentiation generates unstable spatial map orientation and inaccurate navigation. Nat Commun 10:1–13.

Maingret N, Girardeau G, Todorova R, Goutierre M, Zugaro M (2016) Hippocampo-cortical coupling mediates memory consolidation during sleep. Nat Neurosci 19:959–964.

Mano NI (1970) Changes of simple and complex spike activity of cerebellar Purkinje cells with sleep and waking. Science 170:1325–1327.

Marchesi GF, Strata P (1970) Climbing fibers of cat cerebellum: modulation of activity during sleep. Brain Res 17:145–148.

Marks GA, Farber J, Rubinstein M, Roffwarg HP (1980) Demonstration of ponto-geniculo-occipital waves in the albino rat. Exp Neurol 69:648–666.

McCarley RW, Hobson JA (1972) Simple spike firing patterns of cat cerebellar Purkinje cells in sleep and waking. Electroencephalogr Clin Neurophysiol 33:471–483.

Newman PP, Reza H (1979) Functional relationships between the hippocampus and the cerebellum: an electrophysiological study of the cat. J Physiol 287:405–426.

Nicola W, Clopath C (2019) A diversity of interneurons and Hebbian plasticity facilitate rapid compressible learning in the hippocampus. Nat Neurosci 22:1168–1181.

Niedermeyer E, Uematsu S (1974) Electroencephalographic recordings from deep cerebellar structures in patients with uncontrolled epileptic seizures. Electroencephalogr Clin Neurophysiol 37:355–365.

Nitzan N, McKenzie S, Beed P, English DF, Oldani S, Tukker JJ, Buzsáki G, Schmitz D (2020) Propagation of hippocampal ripples to the neocortex by way of a subiculum-retrosplenial pathway. Nat Commun 11:1–17.

Palmer C (1979) Interpositus and fastigial unit activity during sleep and waking in the cat. Electroencephalogr Clin Neurophysiol 46:357–370.

Pellet J, Harley F (1977) Relations between unit activity of the vermis and the phasic waves of the electrocerebellogram during sleep in the chronic cat. Arch Ital Biol 115:108–135.

Ramirez-Villegas JF, Besserve M, Murayama Y, Evrard HC, Oeltermann A, Logothetis NK (2021) Coupling of hippocampal theta and ripples with pontogeniculooccipital waves. Nature 589:96–102.

Rochefort C, Arabo A, Andre M, Poucet B, Save E, Rondi-Reig L (2011) Cerebellum shapes hippocampal spatial code. Science 334:385–389.

Roš H, Sachdev RN, Yu Y, Šestan N, McCormick DA (2009) Neocortical networks entrain neuronal circuits in cerebellar cortex. J Neurosci 29:10309–10320.

Rowland NC, Goldberg JA, Jaeger D (2010) Cortico-cerebellar coherence and causal connectivity during slow-wave activity. Neuroscience 166:698–711.

Saint-Cyr JA, Woodward DJ (1980a) A topographic analysis of limbic and somatic inputs to the cerebellar cortex in the rat. Exp Brain Res 40:13–22.

Saint-Cyr JA, Woodward DJ (1980b) Activation of mossy and climbing fiber pathways to the cerebellar cortex by stimulation of the fornix in the rat. Exp Brain Res 40:1–12.

Schabus M, Dang-Vu TT, Albouy G, Balteau E, Boly M, Carrier J, Darsaud A, Degueldre C, Desseilles M, Gais S, Phillips C, Rauchs G, Schnakers C, Sterpenich V, Vandewalle G, Luxen A, Maquet P (2007) Hemodynamic cerebral correlates of sleep spindles during human non-rapid eye movement sleep. Proc Natl Acad Sci USA 104:13164–13169.

Schwarz C (2010) The fate of spontaneous synchronous rhythms on the cerebrocerebellar loop. Cerebellum 9:77–87.

Siclari F, Tononi G (2017) Local aspects of sleep and wakefulness. Curr Opin Neurobiol 44:222–227.

Servais L, Bearzatto B, Schwaller B, Dumont M, De Saedeleer C, Dan B, Barski JJ, Schiffmann SN, Cheron G (2005) Mono- and dual-frequency fast cerebellar oscillation in mice lacking parvalbumin and/or calbindin D-28k. Eur J Neurosci 22:861–870.

Siapas AG, Wilson MA (1998) Coordinated interactions between hippocampal ripples and cortical spindles during slow-wave sleep. Neuron 21:1123–1128.

Tsunematsu T, Patel AA, Onken A, Sakata S (2020) State-dependent brainstem ensemble dynamics and their interactions with hippocampus across sleep states. Elife 9:e52244.

Velluti R, Yamuy J, Hadjez J, Monti JM (1985) Spontaneous cerebellar nuclei PGO-like waves in natural paradoxical sleep and under reserpine. Electroencephalogr Clin Neurophysiol 60:243–248.

Wang D, Ikemoto S (2016) Coordinated interaction between hippocampal sharp-wave ripples and anterior cingulate unit activity. J Neurosci 36:10663–10672.

Watson TC, Obiang P, Torres-Herraez A, Watilliaux A, Coulon P, Rochefort C, Rondi-Reig L (2019) Anatomical and physiological foundations of cerebello-hippocampal interaction. Elife 8:e41896.

Xu W, De Carvalho F, Clarke AK, Jackson A (2020) Communication from the cerebellum to the neocortex during sleep spindles. Prog Neurobiol 199:101940.

Zhang LB, Zhang J, Sun MJ, Chen H, Yan J, Luo FL, Yao ZX, Wu YM, Hu B (2020) Neuronal activity in the cerebellum during the sleep-wakefulness transition in mice. Neurosci Bull 36:919–931.